Microporous and Mesoporous Materials 304 (2020) 109402

Contents lists available at ScienceDirect

Microporous and Mesoporous Materials

journal homepage: www.elsevier.com/locate/micromeso

Mineralogical alterations in calcite powder flooded with $MgCl_2$ to study Enhanced Oil Recovery (EOR) mechanisms at pore scale

Mona W. Minde[a,b,*], Merete V. Madland[a,c], Udo Zimmermann[a,c], Nina Egeland[a,c], Reidar I. Korsnes[a,c], Eizo Nakamura[d], Katsura Kobayashi[d], Tsutomu Ota[d]

[a] The National IOR Centre of Norway, UiS, PO Box 8600 Forus, 4036, Stavanger, Norway
[b] Department of Mechanical and Structural Engineering and Materials Science, University of Stavanger, 4036, Stavanger, Norway
[c] Department of Energy Resources, University of Stavanger, 4036, Stavanger, Norway
[d] Institute for Planetary Materials, Okayama University, Misasa, Tottori, 682-0193, Japan

ARTICLE INFO

Keywords:
Mineral replacement reactions
EOR
Calcite
FE-SEM
FE-TEM

ABSTRACT

Seawater injection into chalk-reservoirs on the Norwegian Continental Shelf has increased the oil recovery and reduced seabed subsidence, but not eliminated it. Therefore, understanding rock–fluid interactions is paramount to optimize water injection, predict and control water-induced compaction.

Laboratory experiments on onshore and reservoir chalks have shown the need to simplify the aqueous chemistry of the brine, and also the importance of studying the effect of primary mineralogy of chalk to understand which ions interact with the minerals present. In this study, the mineralogy of the samples tested, are simplified. These experiments are carried out on pure calcite powder (99.95%), compressed to cylinders, flooded with $MgCl_2$, at 130 °C and 0.5 MPa effective stress, for 27 and 289 days.

The tested material was analysed by scanning and transmission electron microscopy, along with whole-rock geochemistry. The results show dissolution of calcite followed by precipitation of magnesite. The occurrence and shape of new-grown crystals depend on flooding time and distance from the flooding inlet of the cylinder. Crystals vary in shape and size, from a few nanometres up to 2 μm after 27 days, and to over 10 μm after 289 days of flooding and may crystallize as a single grain or in clusters.

The population and distribution of new-grown minerals are found to be controlled by nucleation- and growth-rates along with advection of the injected fluid through the cores. Our findings are compared with in-house experiments on chalks, and allow for insight of where, when, and how crystals preferentially grow.

1. Introduction

Over the last four decades, large amounts of mechanical flow-through core experiments have been carried out to investigate the effect of injection of seawater-like brines into onshore and reservoir chalk and how these brines affect rock properties and production of hydrocarbons. Declining reservoir pressure and seabed subsidence were experienced at the Ekofisk chalk field in the 1980s, and subsequently, a program of seawater-injection was initiated [1–5]. The reservoir was re-pressurized; however, seabed subsidence could not be completely eliminated. This is believed to be caused by the interplay between the chalk and the ions in the seawater, processes well-known as “water weakening of chalk” [6–17]. There are multiple processes affecting the rock during flooding with reactive brines. This includes changes in surface-complexation, -charge and -potential along with alterations of mineralogy (e.g. Refs. [6,7,10,18–31]). Changes in e.g. mineralogy affect both compaction of chalk as well as wettability of the grain surfaces. Enhanced oil recovery (EOR) is concerned with increasing the recovery of oil by optimizing the injection fluid and control and predict the induced alterations in the most favourable way.

Understanding water weakening of chalk is important to control and predict hydrocarbon-reservoir behaviour in a safe and financially effective manner, and leave an as low as possible environmental footprint. Water weakening also plays a role in carbonate aquifers and erosion of costal carbonate cliff formations [32].

Chalk is a rather simple rock in a mineralogical aspect, with the major constituent being calcite ($CaCO_3$). Additionally, it contains minor occurrences, varying from a few and up to 15 wt% (weight percent), of other minerals such as dolomite, quartz, opal, apatite, feldspar, oxides and different clay-minerals, depending on location, age and degree of

* Corresponding author. The National IOR Centre of Norway, UiS, PO Box 8600 Forus, 4036, Stavanger, Norway.
E-mail address: mona.w.minde@uis.no (M.W. Minde).

https://doi.org/10.1016/j.micromeso.2019.03.050
Received 30 May 2018; Received in revised form 15 March 2019; Accepted 29 March 2019
Available online 01 April 2019

diagenesis [33]. Chalk is characterized as a fine-grained sedimentary rock, built mainly of skeletal debris of calcareous micro-fossils such as coccolithophores, calcispheres, foraminifera along with fragments of macrofossils [33]. The differences in structure, size and primary composition of the fossils seem to have an effect on the alteration-pattern when chalk is exposed to reactive brines [34]. Additionally, even though chalk largely consists of calcite, differences in primary mineralogy dictate many of the alterations found during mechanical flow-through experiments, revealing an extraordinary complex rock-fluid interaction. The need for simplification of the system has therefore become necessary, where e.g. the injected $MgCl_2$ represents the simplified aqueous chemistry of seawater, to specifically study the effect of the Mg^{2+}-ions. Even though small effects of ion-exchange have been observed, the main alterations found in chalk by injection of $MgCl_2$-brine are; dissolution of calcite ($CaCO_3$) and precipitation of magnesite ($MgCO_3$) [10,22,29,30,35,36].

To simplify the system even further, chalk has in this study been replaced with pure calcite powder (99.95% $CaCO_3$). Numerous experiments have been carried out on single calcite crystals to study changes in mineralogy on nano- and micro-scale, when exposed to non-equilibrium brines (e.g. by AFM, review in Ref. [37]). This study aims to investigate how the mineralogical changes in porous multi-grain calcite systems are affected by time and distance from injection-point. These observations are paramount as input parameters for simulation and modelling of EOR-experiments on all scales, from pore (μm) to field (km).

2. Materials and methods

2.1. Calcite powder

The calcite powder was manufactured by Merck®, and consists of 99.95% calcite ($CaCO_3$). Minor impurities of other elements such as Fe and Mg occur, however the total adds up to only ~0.05%. The particle size is given as an average of ~14 μm, ranging from 3 to 44 μm. Before use, the powder was dried over night at 60 °C in a heating cabinet and packed into heat-shrinkage tubing and compressed to cylinders (D ~ 3.7 cm, L ~ 7.0 cm) (Fig. 1), hereafter referred to as "artificial chalk cores". One core, named "CORE 1", was flooded for 27 days, while the other core, "CORE 2", was flooded for 289 days.

2.2. Triaxial tests

The two artificial chalk cores, produced from calcite powder, were in each end of the shrinkage tubings fitted with drainage plates, and 8 μm filters. The cores were then mounted into triaxial cells which allow for flow-through experiments at elevated pressures, stresses and temperatures. The cells were equipped with heating jackets that kept the temperature constant at 130 ± 0.1 °C. A pore pressure of 0.7 MPa was applied by the use of a back pressure regulator, to avoid boiling of the pore fluids at temperatures over 100 °C. For a complete description of the set-up, the reader is referred to Ref. [29].

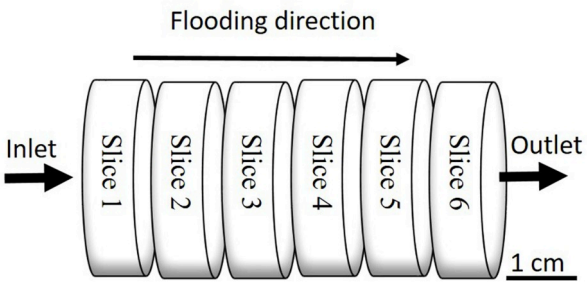

Fig. 1. Sketch of the artificial cores and how the cores were split after the tests for analyses.

Both cores were injected with at least three pore volumes (PV) of distilled water (DW) during the first 24 h of the test to clean the pore system. During these 24 h, the pore pressure and the confining pressure were increased from 0 to 0.5 MPa, to 0.7 and 1.2 MPa, respectively, and thereby producing an effective stress of 0.5 MPa, before the test temperature was increased to 130 °C.

After the initial phase, 0.219 M $MgCl_2$ was introduced as flooding-brine and the flooding rate was reduced to approximately one pore volume per day. The initial pore volumes were calculated based on geometry, weight and density of each core, and yielded a flooding rate of 0.022 ml/min for CORE 1 and 0.025 ml/min for CORE 2.

After the end of the two experiments, the cores were cleaned with at least three pore volumes of DW to remove ions in the pore-fluid, which could precipitate after the end of the tests. Both cores were dried in heating cabinets at ~60 °C until stable weight to ensure a dry sample before further analyses.

During the experiments, the effluents were regularly collected, and the composition analysed by ion chromatography (results not shown here).

2.3. Inductive Coupled Plasma-Mass Spectroscopy (ICP-MS)

Representative sample material was retrieved along the flooding axis of each of the two artificial chalk cores (Fig. 1). For CORE 1, flooded for 27 days, the material was not sufficiently consolidated after flooding to be cut into slices, however, material from the entire radius of the core was attempted sampled to produce material for ICP-MS analyses (~5 g). For CORE 2, flooded for 289 days, the powder was sufficiently consolidated to be cut into six slices, where half of each slice was used for ICP-MS analyses. Only the last approximate centimetre at the outlet was still unconsolidated. Sampling of the powdered part of the cores may introduce errors in measurements as it is challenging to produce a sample representative of the entire radius of the core.

The material was milled and analysed at Bureau Veritas Minerals' laboratories in Canada with a porcelain beaker to avoid any contamination. Details for the analytical method and processing can be found in http://acmelab.com, but is compiled here: The samples were ground in an agate mill. The milled sample was then mixed with $LiBO_2$/$Li_2B_4O_7$ flux in crucibles and fused in a furnace. The cooled bead was dissolved in ACS grade nitric acid and analysed by ICP-MS. Loss on ignition (LOI) was determined by igniting a sample split then measuring the weight loss. A 1 g sample was weighed into a tarred crucible and ignited to 1000 °C for 1 h, and then was cooled and weighed again. The loss in weight is the LOI of the sample. Total Carbon and Sulphur were determined by the Leco method. Here, induction flux was added to the prepared sample then ignited in an induction furnace. A carrier gas sweeps up released carbon to be measured by adsorption in an infrared spectrometric cell. Results are total concentrations and attributed to the presence of carbon and sulphur in all components. An additional 14 elements were measured after dilution in Aqua Regia. The prepared sample was digested with a modified Aqua Regia solution of equal parts concentrated HCl, HNO_3, and DI-H_2O for 1 h in a heating block or hot water bath. The sample volume was increased with dilute HCl-solutions and splits of 0.5 g were analysed. None of the measured concentrations was too far above the possible detection limit, but in standard range, and accuracy and precision are between 1 and 2%.

2.4. Field Emission Scanning Electron Microscopy (FE-SEM) combined with energy dispersive spectroscopy (EDS)

FE-SEM was performed on selected samples from each core using a Zeiss Supra 35VP at the University of Stavanger. Between 5 and 15 kV acceleration voltage was used, with an aperture of 30 or 60 μm and working distance between 3 and 15 mm. For Energy dispersive x-ray spectroscopy (EDS), an EDAX detector was used. To optimize the quantification results, an Iceland spar calcite or Astimex dolomite were

used as standards to calibrate the EDS system. To ensure a steady flux of electrons, the samples were coated with palladium (Pd).

2.5. Field Emission Transmission Electron Microscopy (FE-TEM) combined with energy dispersive spectroscopy (EDS)

A FE-TEM, JEOL JEM-2100F, housed at the Institute for Planetary Materials (IPM) Okayama University, Misasa, Japan, was used for investigation of the artificial chalk cores after flooding. Specimen preparation for FE-TEM investigations were preformed using a focused ion beam (FIB) technique with a JEOL JIB-4500 system (FIB-SEM) equipped with a gallium (Ga) ion-gun. The areas selected for investigation were carbon-coated by ion-beam assisted deposition. To produce the extreme thin samples needed for FE-TEM analyses, a Ga ion-beam at 30 kV was used to mill the samples into ~150 nm thin slices. Prepared slices were transferred to perforated carbon film on a copper grid by the use of manipulators. Each FIB-slice was mapped using scanning transmission electron microscopy mode (STEM), performed with an accelerating voltage of 200 kV, beam current of 2.6 nA, dwell time of 0.2 ms. Mapping by energy dispersive X-ray spectroscopy (EDS) was performed, where the resolution of the maps was set to 1 pixel = 5.8 nm. Additionally, EDS line-scans were performed, to create profiles of calcium- and magnesium-content over cross-sections of crystals.

3. Results

3.1. General properties of the cores after flooding

After testing both cores were dried inside the heat-shrinkable tubing they were assembled in. After the cores reached a stable weight, the sleeve was carefully cut to collect samples for analyses. CORE 1 was difficult to sample, due to the lack of consolidation throughout the core. CORE 2, on the other hand, had solidified through most of the core, except for the approximate last cm.

The waste-water, or effluent, were collected from the outlet of the two cores during the experiments. The results are not presented here, but in general, the calcium and magnesium profiles follow similar trends as with outcrop chalk experiments (e.g. Refs. [10,29,30,36]), where Mg^{2+}-ions are retained in the core and Ca^{2+}-ions are enriched in the effluent compared to the injected brine.

3.2. Inductive Coupled Plasma-Mass Spectroscopy (ICP-MS)

Both cores were sampled along the flooding axis of the cylinder, split in "slices" approximately 1 cm thick (Fig. 1). Table 1 shows that for all samples of the flooded cores, the MgO content has increased compared to unflooded material (0.02 wt%; where wt indicates weight). Except for slice 1, CORE 1, there is a decreasing trend in MgO content from the inlet to the outlet of the two cores, varying from 0.93 wt% in slice 2 to 0.03 wt% in slice 6 for CORE 1 and 32,88 wt% in slice 1 and 0.24 wt% in slice 6 for CORE 2. This is accompanied by an inverse trend in the CaO concentrations, reaching as low as 18.02 wt% in slice 1, CORE 2. The MgO values are, not surprisingly, more enriched after 289 days of flooding than after 27 days.

The MgO value for slice 1, CORE 1 is lower than in slice 2. This is in line with previous studies where the peak in MgO content was found in slice 2 for several types of outcrop chalk [29].

3.3. Field Emission Scanning Electron Microscopy (FE-SEM)

Samples from selected areas of each core were prepared for analyses, focusing on the centre of each core, moving from inlet to the outlet along the flooding axis (Fig. 1). For comparison, samples of unflooded calcite powder were also imaged.

Unflooded material match well the description from the manufacturer, with grains varying in size between 4 and 33 μm. Crystals display trigonal crystal shape, often with grains interlocking (Fig. 2 a and b). Grain surfaces are clean and no other elements other than carbon, oxygen and calcite were detected by EDS.

Table 1
Results of ICP-MS analyses of the two flooded cores, along with the values for unflooded powder. Only the wt% for MgO and CaO are presented.

CORE 1, flooded for 27 days		
Analyte	MgO wt%	CaO wt%
Detection limit	0.01	0.01
CORE 1_slice 1	0.38	56.10
CORE 1_slice 2	0.93	55.50
CORE 1_slice 3	0.97	55.52
CORE 1_slice 4	0.67	55.88
CORE 1_slice 5	0.34	56.34
CORE 1_slice 6	0.03	56.81
Unflooded (both cores)	0.02	56.20
CORE 2, flooded for 289 days		
Analyte	MgO wt%	CaO wt%
Detection limit	0.01	0.01
CORE 2_slice 1	32.88	18.02
CORE 2_slice 2	13.31	40.73
CORE 2_slice 3	7.36	47.57
CORE 2_slice 4	3.26	52.57
CORE 2_slice 5	1.40	54.34
CORE 2_slice 6	0.24	55.53

In flooded material three main alteration-stages are observed. The first stage can be seen in the inlet of CORE 1, flooded for 27 days, Fig. 3. The observations include angular grains with trigonal crystal shape varying in size from only tens of nm to ~2 μm. These crystals grow on top of existing calcite grains and the edges of the crystals are often incomplete, interpreted as step-wise crystal growth. Accurate EDS analyses of these crystals are challenging in FE-SEM because of the small crystal size compared to the beam-size. However, analyses show a significant content of magnesium (not shown here).

The original calcite grains show defects on the crystal surfaces (Fig. 3), not observed in unflooded material (Fig. 2), where the high magnesium crystals grow. Other crystals faces appear smooth without any new-growth (Fig. 3b).

The second stage of alteration is only observed in CORE 2, flooded for 289 days. Polycrystalline aggregates with high magnesium content are found growing between larger calcite crystals (Fig. 4). The clusters comprise of idiomorphic crystals with a trigonal crystal shape and sizes varying between 100 and 200 nm. The clusters themselves vary in size, most often between 2 and 5 μm, and display a framboidal shape, similar to what can be found for pyrite [38]. Despite the small individual crystal size, EDS measurements of the clusters display a convincing amount of magnesium in the crystals (Fig. 4c). The clusters are abundant in the middle section of CORE 2, approximately halfway between the inlet and the outlet (Fig. 1).

Also in the second stage, found in CORE 2, severe signs of dissolution are observed on calcite grains (Fig. 5). The dissolution is seen as defects on the crystal faces, where layers in the crystals are partly absent. The surfaces of some of the crystals in Fig. 5 (marked by white, dashed boxes) were analysed by EDS, and no magnesium was present on the structures left on the surfaces. This indicates that the defects are signs of dissolution of calcite, and not precipitation of magnesite.

At the outlet of CORE 2, similar polycrystalline aggregates are found, however of smaller size (Fig. 6). The size of the clusters varies between ~100 nm and 2 μm, and the occurrence is scarce. EDS analyses indicate a high magnesium concentration, however, the clusters are in this case too small to produce an accurate result.

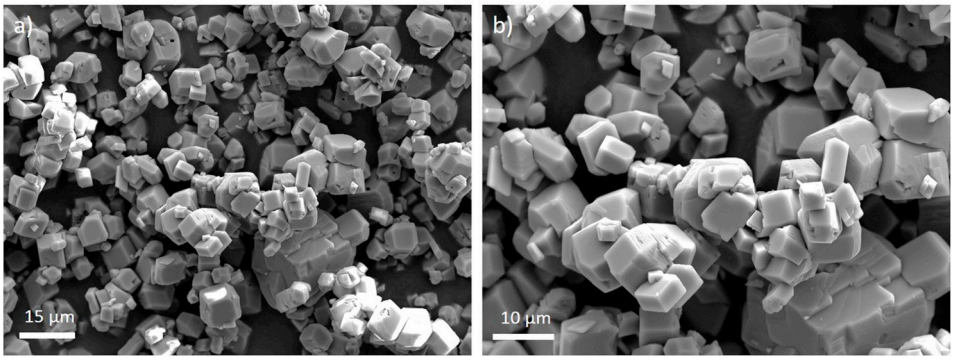

Fig. 2. FEG-SEM micrographs of unflooded calcite powder at two different magnifications a) and b). Grain-size vary between ~4 and 33 µm, with partially interlocking grains.

The last observable stage is found at the inlet of CORE 2, where most of the crystals found only millimetres from the inlet, contain a high amount of magnesium (Fig. 7). The crystals are in different sizes and shapes, mainly with a bimodal distribution:

- Smaller angular crystals with a size below 2 µm
- Larger crystals in the size-rage between 10 and 15 µm with irregular shapes, partly rounded.

At least one of the faces of the larger crystals are smooth, while other directions have rough surfaces. EDS analyses of all grains in this area show next to no content of calcium, with the major ion constituents C, O and Mg (Fig. 7 c). The composition based on the EDS analyses allows for the interpretation that the new-grown mineral is magnesite, and the high magnesium carbonate crystals will hereafter be referred to as magnesite.

3.4. Field Emission Transmission Electron Microscopy (FE-TEM)

To verify the composition and nature of growth of the magnesite crystals, FIB-slices of the samples were analysed by STEM-EDS [39]. Fig. 8a and b shows a bright field image of a magnesite crystal precipitated on top of a calcite crystal along with STEM-mapping of calcium- and magnesium-distribution in the two crystals. The FIB-lamella was prepared from the inlet of CORE 1. As can be seen in both Fig. 8a and b, the transition between the two adjacent crystals is sharp. The Ca- and Mg-concentrations in both crystals were scanned over a cross-section in Fig. 8c and d. The distribution of Mg and Ca is uniform within the two crystals in the line-scan, and nearly no gradual transition between the two phases is observed. The area where Ca decreases and Mg increases is less than 50 nm wide. Only minor impurities of calcium can be found homogenously distributed within the magnesite crystal.

4. Discussion

The analyses presented in this study clearly show that alterations from calcite to high magnesium carbonate or magnesite are not uniform throughout the flooded artificial chalk cores. FE-TEM studies (Fig. 8) show that processes of alteration are linked to dissolution and precipitation, and not to solid-state molecular diffusion, as the transitions between the Ca- and Mg-distribution in crystals are rather abrupt. For magnesite to crystallize, the pore-fluid needs to be super-saturated with regard to magnesite. The degree of super-saturation plays a role dictating crystal growth and nucleation rates [40,41]. These rates affect the distribution in crystal size and population. Differences in flow rate may also affect the growth rate of crystals. The experiments carried out in this study, were performed at 130 °C, but at rather low pressures (effective stresses of 0.5 MPa). This excludes effects of pressure solution or consolidation due to compaction. As such, the consolidation seen in CORE 2 can be attributed to mineralogical alterations alone. As the last centimetre of the outlet of CORE 2 is not consolidated and CORE 1 is not consolidated at all, we draw the conclusion that these mineralogical alterations progress as a front from the inlet towards the outlet over time in such experiments, confirming observations studying onshore chalks [35]. Based on ICP-MS analyses, the amount of precipitation of magnesite needed to consolidate the core seemingly has to be higher than the values found in CORE 1 and slice 6 of CORE 2, corresponding to 0.97 wt% MgO, Table 1.

In the flooded cores, we observed three different stages of dissolution and precipitation. The major difference between the stages are: 1) the abundance of calcite and 2) the size and shape of the precipitated magnesite crystals. Temperature and mass transfer are similar throughout the core during the experiments. Thus, the factor affecting the driving force conditions for dissolution and precipitation is the degree of super-saturation, i.e. how far from thermodynamic

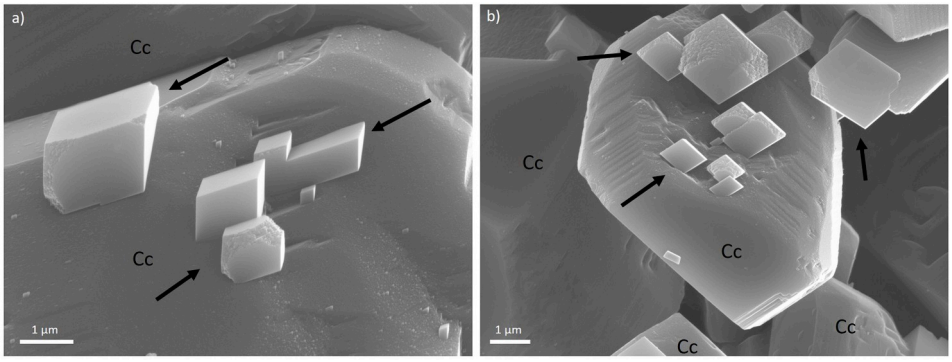

Fig. 3. FEG-SEM micrographs of crystals with high magnesium content growing on existing calcite grains at the inlet of CORE 1, marked with black arrows. Original calcite grains are marked with Cc.

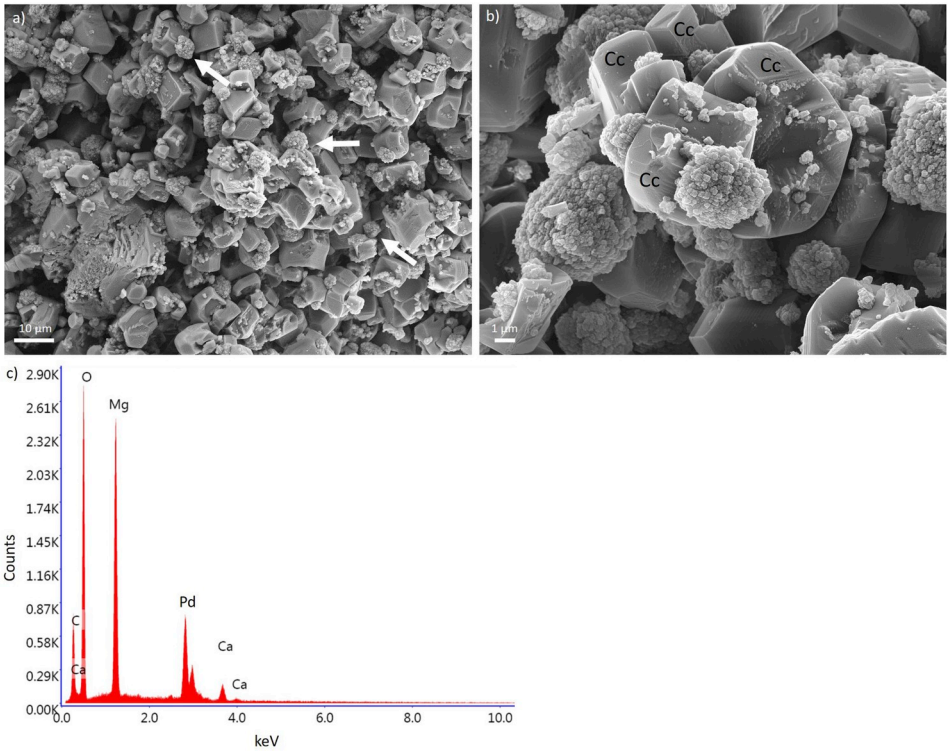

Fig. 4. FEG-SEM micrograph of clusters of new-grown crystals with high magnesium content. White arrows point to some of these clusters in a); b) shows a close-up of the clusters. Original calcite grains are marked with Cc. These observations are made halfway along the flooding-axis of CORE 2. c) EDS spectrum of the clusters of new-grown minerals with main contents of C, O and Mg and only minor content of Ca.

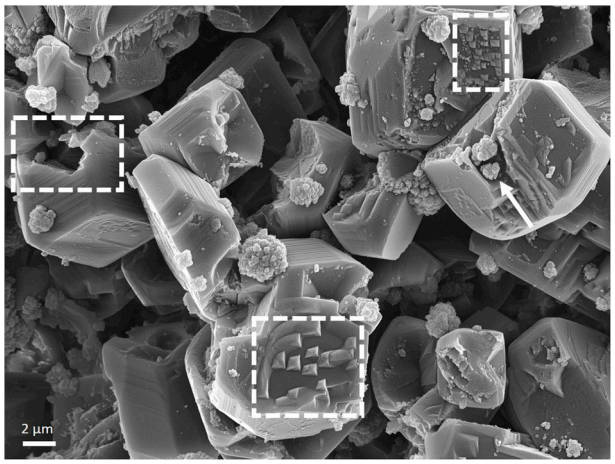

Fig. 5. Severe defects on crystal faces found in CORE 2, halfway between the inlet and the outlet of the cylinder. White boxes show partly dissolved surfaces, while the white arrow point to polycrystalline magnesium aggregates inside one of the defects.

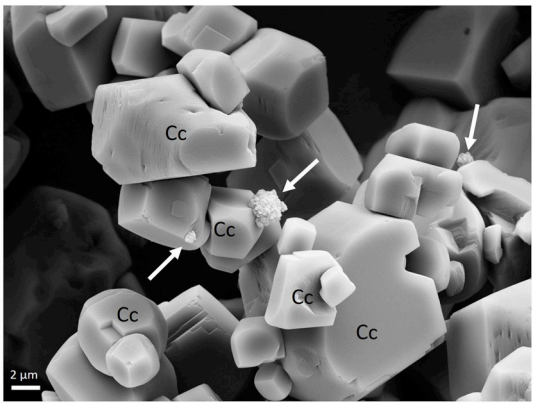

Fig. 6. Polycrystalline aggregates of magnesite placed on the top of calcite grains at the outlet of CORE 2 indicated by white arrows, all other grains are calcite, main marked with Cc.

equilibrium the system is. The differences in crystals shape, size and assemblage may be linked to how large the driving force conditions were during precipitation.

In the primary stage of precipitation, observed close to the inlet of CORE 1 after only 27 days, single, µm-sized and below, magnesite crystals precipitate on top of existing calcite grains. Such crystals commonly form due to conditions of low super-saturation, with favourable growth rates compared to nucleation rates [41]. Halfway along the flooding axis of CORE 2, framboidal polycrystalline aggregates of smaller magnesite crystals are observed, often associated with higher degree of super-saturation, where the nucleation rate is higher than the growth rate. However, these findings are contradictive to the saturation indexes calculated for mechanical flow-through on-shore chalk experiments, where a gradient is expected from the inlet towards the outlet with a decreasing trend in the degree of super-saturation [42]. This is confirmed by the distribution of magnesium-bearing minerals formed during flooding, peaking near the inlet, with a gradual decrease in magnesium concentration towards the outlet (e.g. Refs. [29,36]). A similar trend in magnesium concentration is also observed by ICP-MS for these artificial chalk experiments, and suggests higher degrees of chemical alteration at the inlet than at the outlet. Hence, the population and shape of the precipitated magnesite crystals distributed along the flooded artificial chalk cores must be explained by a different mechanism. As the super-saturation of magnesite is highest near the inlet inducing a high nucleation rate, precipitation of magnesite crystals may also take place in the fluid-phase [43]. Nanometre-sized crystals can then be transported by advection in the cores and aggregate during transport as also modelled as gelation processes in sodium silicate polymers [44]. When these aggregates reach a certain size, transport through the fine-grained pore-network is no longer possible, and the aggregates settle on calcite grains further toward the outlet of the cores. Simultaneously, crystals already precipitated onto calcite grains in the inlet continue to grow, forming larger sized single

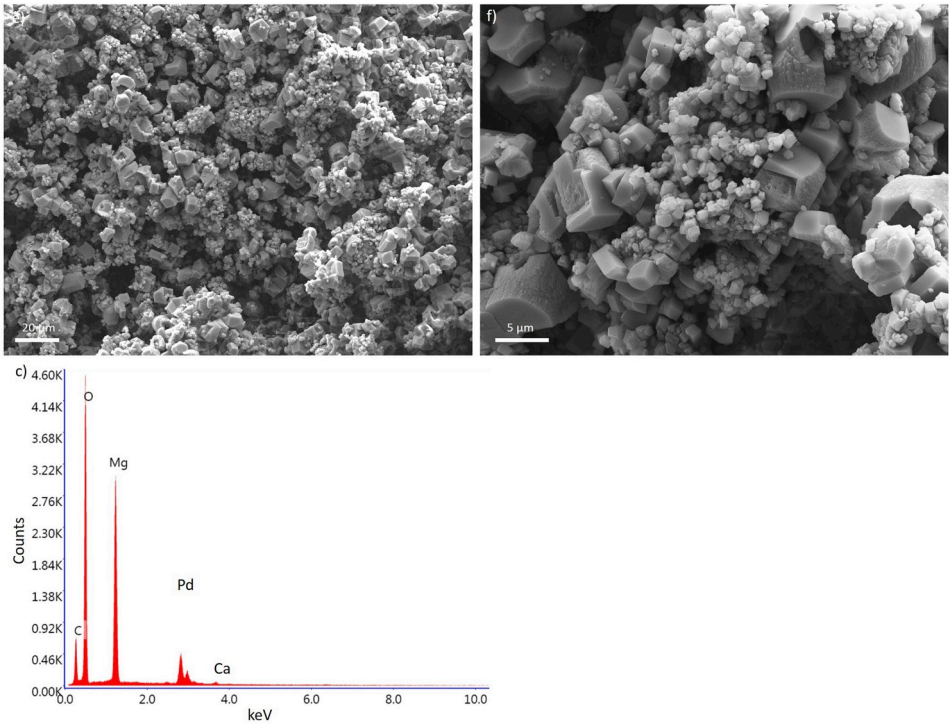

Fig. 7. FEG-SEM micrographs of the third stage of mineralogical alteration. A distribution of crystals of different sizes and shapes is observed. All grains show minimal content of Ca, a typical EDS spectrum shown in c), samples coated with palladium (Pd).

crystals. The abundance of magnesite and calcite at any given time and point in the core will influence the dissolution or precipitation rate accordingly, along with the surface properties of grains and crystals. As such, a combination of nucleation rate, growth rate and advection controls the distribution and population of magnesite and calcite crystals in the flooded artificial chalk cores. A certain degree of transportation is also in line with that the peak in the MgO concentration, measured by ICP-MS, for CORE 1 is not observed at the first slice, but further into the core. This has also been observed in tests on onshore chalk [29]. The trend in CORE 1is contradictory to CORE 2, where the MgO peak is found at the very inlet. This pattern of alteration is the same as observed in long-term-tests of onshore chalk, where a front of complete alteration to magnesite progressing from the inlet towards the outlet is observed [35].

In the artificial chalk core flooded for 289 days, large areas of the core are completely transformed from calcite to magnesite, with varying crystal-sizes. Similar observations are made in long-term-test of flooded outcrop chalk from Liège (Belgium). These cores were flooded with 0.219 M $MgCl_2$, as in this study, and for two cores, flooded for 516 and 718 days, the areas towards the inlet of the cores are completely altered to magnesite [35].

After short periods of flooding outcrop chalks, single magnesite crystals are precipitated towards the inlet of the cores, but often with sizes up to ~6 µm. These larger crystals are found in large pore-spaces originating from larger microfossils, such as foraminifera (e.g. Refs. [29,45]). The difference in crystals size in onshore chalk, compared to what is found in artificial chalk (CORE 1) may be attributed to the difference in original pore-space for crystals to grow in. However, the driving force conditions may also be influenced by changes in flow-rates and super-saturation caused by differences in original composition, shape, size and permeability of the porous medium. The framboidal aggregates found in artificial chalk from calcite powder are also found in flooded outcrop chalk towards the outlet side of the cores.

When comparing outcrop chalks to the here presented artificial cores, the major difference is how the original texture of the chalk affects the mineralogical alteration, both with regards to crystal size and distribution. In the artificial chalk, the composition, size and shape of the calcite crystals are considered homogenous, unlike e.g. the different fossils found in outcrop chalk, with varying MgO/CaO ratios and shell compositions, which impact the mineralogical alterations [34]. However, the type of mineral and the resulting textures after flooding with $MgCl_2$ are similar for both the artificial and onshore chalk, and the findings in this study can thus be used to understand mineralogical alterations in onshore and reservoir chalks and subsequently how these alterations impact the mechanical parameters of chalks.

The results from these simplified experiments cannot be directly used to explain reservoir rock behaviour or core-scale experiments of reservoir rock or analogues. However, they elucidate the mechanisms that govern the mineralogical alterations which occur in these setting, and should be incorporated in computational engineering to build sound models of experiments or alterations in a reservoir. Several observations have been made which impact simulation and modelling of EOR-experiments at all scales: 1) Mineral transformation from calcite to magnesite happens through dissolution and precipitation, not by solid state molecular diffusion, as observed by FE-TEM studies (Fig. 8). 2) Nanometre sized crystals are precipitated in the fluid phase and transported together with ions throughout the porous medium. This is based on the expected crystal shape and size related by the calculated saturation indices in mechanical flow-through experiments on outcrop chalk. 3) Texture, i.e. size of fractures, fossil assemblage and cementation of the rock are controlling the position and type of replacement, and need to be included in numerical modelling.

The experiments in this study have been performed on simplified core samples. The next step would be to introduce other minerals to the calcite powder to match closer the mineralogy of reservoir rocks. By studying simplified systems, it is possible to observe the impact of each single phase – and the impact of mineral-mineral interactions - allowing for evaluation of the impact of each of the phases during complex rock–fluid interactions and its final contribution to the alteration of the rock. Additionally, more realistic geometries should be produced to understand the effects of the texture of the rock, where one possibility may be additive manufacturing using mineral powders.

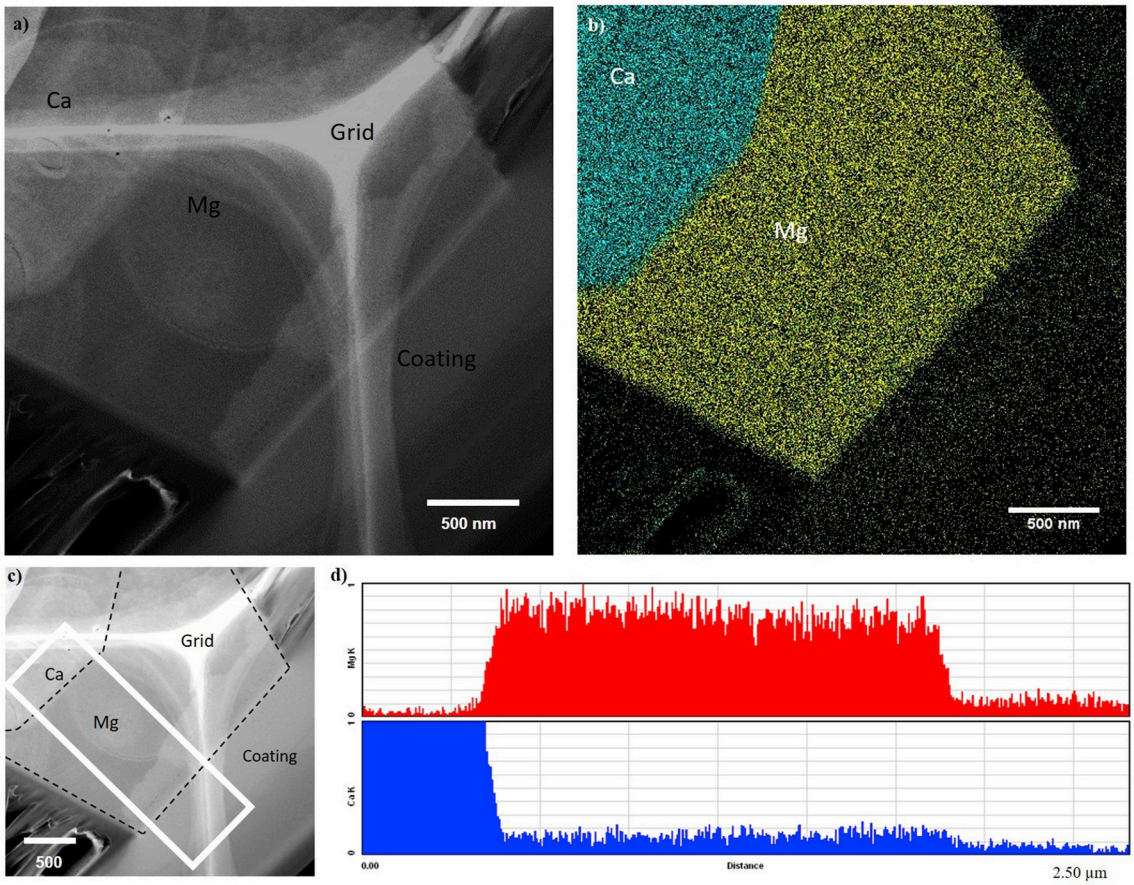

Fig. 8. a) Bright field image of adjacent crystals. b) STEM mapping of crystal growing on top of original calcite crystal at the inlet of CORE 1. Ca = calcium = blue, Mg = magnesium = yellow. c) Shows the position of the line-scan profiles for the crystals in a). d) Demonstrates the chemical analysis along the line scan in c) with X-ray intensities for Mg and Ca. The white pattern behind the crystals is the copper grid the slice is attached to. Ca = calcium = blue, Mg = magnesium = red. (For interpretation of the references to colour in this figure legend, the reader is referred to the Web version of this article.)

5. Conclusion

The presented study of flooding experiments on calcite powder shows that in high-temperature (130 °C) advective flooding with 0.219 $MgCl_2$, the population and size distribution of precipitated magnesite crystals are not uniform along the flooding axis of the cores. Both single crystals up to two µm in size are present along with polycrystalline aggregates in the form of framboids. The distribution of these different stages does not match the saturation indexes calculated for such experiments. It is feasible to assume that transport of nanometre-sized crystals precipitating in the fluid-phase engages in a paramount role in this mineral-fluid interplay. As such, a combination of nucleation rate, growth rate and advection within the core controls the crystal shape and size of newly formed magnesite.

Similar crystal observations have been attained in flooded outcrop chalk, and a theory of transportation of minute magnesite crystals through the cores also fits well with the behaviour in such cores. The main difference when comparing mineralogical alterations in artificial and outcrop chalk is how the original texture and depositional environment affect the alteration in outcrop chalks, the effect is absent in artificial samples.

Based on these observations, the results of this study can be used to understand the basic mineralogical alteration in calcite-rich materials and link these to changes in geomechanical behaviour.

Acknowledgement

The authors acknowledge the Research Council of Norway and the industry partners, ConocoPhillips Skandinavia AS, Aker BP ASA, Vår Energi AS, Equinor ASA, Neptune Energy Norge AS, Lundin Norway AS, Halliburton AS, Schlumberger Norge AS, Wintershall Norge AS, and DEA Norge AS, of The National IOR Centre of Norway for support.

We like to thank reviewers for their comments and are grateful to the kind and constructive handling of the editor Wolfgang Schmidt. In addition, the authors would like to thank Prof Aksel Hiorth for fruitful discussions. The research presented is integral part of the PhD thesis of Mona Wetrhus Minde.

References

[1] L.W. Teufel, D.W. Rhett, H.E. Farrell, American Rock Mechanics Association, (1991).
[2] N.B. Nagel, Society of Petroleum Engineers, (1998).
[3] Hermansen, H., et al. 2000. p. 11-18.
[4] H. Hermansen, et al., Society of Petroleum Engineers, (1997).
[5] V. Maury, J.M. Piau, G. Halle, SPE European Petroleum Conference, 1996 (Milan, Italy).
[6] T. Heggheim, et al., J. Pet. Sci. Eng. 46 (2005) 171–184.
[7] R.I. Korsnes, et al., J. Pet. Sci. Eng. 60 (3) (2008) 183–193.
[8] M.V. Madland, et al., J. Pet. Sci. Eng. 51 (3–4) (2006) 149–168.
[9] Madland, M.V., et al. 2008: (Abu Dhabi.
[10] M. Madland, et al., Transport Porous Media 87 (3) (2011) 679–702.
[11] R. Risnes, et al., Tectonophysics 370 (2003) 213–226.
[12] M.V. Risnes, et al., J. Pet. Sci. Eng. 48 (1–2) (2005) 21–36.
[13] Hellmann, R., et al. Vol. 7. 2002.
[14] D.W. Rhett, C.J. Lord, American Rock Mechanics Association: Washington, D.C, (2001).
[15] Carles, P. and P. Lapointe, 2005.
[16] Newman, G.H., 1983.
[17] M. Gutierrez, L.E. Øino, K. Høeg, Rock Mech. Rock Eng. 33 (2) (2000) 93–117.
[18] A. Hiorth, L.M. Cathles, M.V. Madland, The Impact of Pore Water Chemistry on

Carbonate Surface Charge and Oil Wettability vol. 85, (2010), pp. 1–21 (1).
[19] A. Hiorth, et al., Geochem. Cosmochim. Acta 104 (2013) 99–110.
[20] M. Megawati, A. Hiorth, M.V. Madland, Rock Mechanics and Rock Engineering, (2012), pp. 1–18.
[21] P. Zhang, M.T. Tweheyo, T. Austad, Colloid. Surf. Physicochem. Eng. Asp. 301 (1) (2007) 199–208.
[22] W. Wang, et al., Geological Society, London, Special Publications, (2016), p. 435.
[23] M. Jackson, D. Al-Mahrouqi, J. Vinogradov, Sci. Rep. 6 (2016) 37363.
[24] J.K. Borchardt, T.F. Yen, A. Chemical Congress of North, ACS Symposium Series, vol. 396, American Chemical Society, Washington, DC, 1989.
[25] T. Austad, et al., SPE Reservoir Eval. Eng. 11 (4) (2008) 648–654.
[26] E. Flügel, Springer, Berlin, 2004.
[27] S. Strand, E.J. Hognesen, T. Austad, Colloid. Surf. Physicochem. Eng. Asp. 275 (1–3) (2006) 1–10.
[28] M.E. Tucker, V.P. Wright, J.A.D. Dickson, Blackwell, Oxford, 1990.
[29] P.Ø. Andersen, et al., Transport in Porous Media, (2017), pp. 1–47.
[30] A. Nermoen, et al., J. Geophys. Res.: Solid Earth 120 (5) (2015) 2935–2960.
[31] E.W. Al-Shalabi, K. Sepehrnoori, J. Pet. Sci. Eng. 139 (2016) 137–161.
[32] J.A. Lawrence, et al., Geomorphology 191 (2013) 14–22.
[33] M.L. Hjuler, I.L. Fabricius, J. Pet. Sci. Eng. 68 (3) (2009) 151–170.
[34] M.W. Minde, et al., Snowmass Colorado, (2016).
[35] M.W. Minde, et al., Stavanger, (2017).
[36] U. Zimmermann, et al., AAPG (Am. Assoc. Pet. Geol.) Bull. 99 (5) (2015) 791–805.
[37] J.W. Morse, R.S. Arvidson, Earth Sci. Rev. 58 (1) (2002) 51–84.
[38] H. Ohfuji, D. Rickard, Earth Sci. Rev. 71 (3) (2005) 147–170.
[39] N. Egeland, et al., Stavanger, (2017).
[40] I. Sunagawa, Cambridge University Press, New York, USA, 2005.
[41] A. Myerson, A.S. Myerson, Butterworth-Heinemann, Boston, 2002.
[42] P.Ø. Andersen, et al., Chem. Eng. Sci. 84 (2012) 218–241.
[43] Z. Sawlowicz, Geol. Rundsch. 82 (1) (1993) 148–156.
[44] A.V. Omekeh, et al., European Association of Geoscientists and Engineers, (2017), p. 17.
[45] M.W. Minde, Wenxia Wang, Merete V. Madland, Udo Zimmermann, Reidar I. Korsnes, Silvana R.A. Bertolino, Pål Ø. Andersen, J. Pet. Sci. Eng. (2018) 454–470.